

Journal of Photonics for Energy

PhotonicsforEnergy.SPIEDigitalLibrary.org

Light-controlled spintronic device based on hybrid organic–inorganic perovskites

Jingying Wang
Xin Pan
Chuang Zhang
Hangwen Guo
Zeev Valy Vardeny

SPIE.

Jingying Wang, Xin Pan, Chuang Zhang, Hangwen Guo, Zeev Valy Vardeny, “Light-controlled spintronic device based on hybrid organic–inorganic perovskites,” *J. Photon. Energy* **8**(3), 032207 (2018), doi: 10.1117/1.JPE.8.032207.

Light-controlled spintronic device based on hybrid organic–inorganic perovskites

Jingying Wang,^a Xin Pan,^a Chuang Zhang,^a Hangwen Guo,^b and Zeev Valy Vardeny^{a,*}

^aUniversity of Utah, Department of Physics and Astronomy, Salt Lake City, Utah, United States

^bLouisiana State University, Department of Physics and Astronomy, Baton Rouge, Louisiana, United States

Abstract. We have fabricated a spin photovoltaic device composed of a vertical spin-valve based on hybrid organic–inorganic perovskite as a spacer layer, of which resistance may be tuned by external light illumination. The magnetoconductivity of this device may be tuned from zero to reach exceptionally high values of 100 k% by controlling the illumination intensity close to the open circuit voltage. In addition, the device photocurrent can be also turned by sweeping the external magnetic field when the effects of the light intensity and applied bias voltage are judiciously balanced. © 2018 Society of Photo-Optical Instrumentation Engineers (SPIE) [DOI: [10.1117/1.JPE.8.032207](https://doi.org/10.1117/1.JPE.8.032207)]

Keywords: hybrid organic–inorganic perovskites; spintronics; photovoltaics.

Paper 18030SS received Feb. 8, 2018; accepted for publication Mar. 30, 2018; published online Apr. 20, 2018.

1 Introduction

Hybrid organic–inorganic perovskites (HOIPs) have attracted a lot of research interest in the past few years because of their promising photovoltaic device applications.^{1,2} As a class of semiconductor, HOIPs exhibit large absorption coefficient, high carrier photogeneration efficiency, and relatively high carrier mobility.^{3–6} These properties lead to photovoltaic devices with power conversion efficiency approaching 22%.³ Moreover, their low-temperature solution-based processing provides simplicity and tunability for device fabrication.⁷ All these advantages make the HOIP strong candidate to play an important role in the semiconductor optoelectronic industry. In addition, fields other than optoelectronics have become a hot topic for research. Recently, the extraordinary spintronic properties of HOIPs have been theoretically advanced and experimentally verified.^{8,9} Due to lack of inversion symmetry and large spin-orbit coupling (SOC) caused by heavy metal and halogen atoms, HOIPs show large Rashba splitting in both conduction band and valence band.¹⁰ In addition, large spin relaxation time has been measured in HOIPs.^{11,12} Consequently, HOIP applications in spintronic device such as spin valve have become an emerging research subject. However, thin film devices based on solution-processed HOIPs suffer from the same problems as other polycrystalline or amorphous films, which are pinholes, impurities, or traps that can largely disturb spin transport in the semiconductor layer and therefore decrease the obtained magnetoresistance in spin valves.¹³

In order to improve the performance of spintronic devices, interplay between electrically injected spin current and photocurrent has been proposed and conducted in devices based on several organic and inorganic semiconductors.^{14–16} Upon illumination, the semiconductor resistance in the spin-valve interlayer can be downtuned by the photogenerated carriers and, consequently, increase the effective magnetoresistance of the device. Due to their excellent optoelectronic properties, as well as spintronic properties, HOIPs may be very effective as the active interlayer in such spin photovoltaic devices. By balancing the photocurrent with the electrically injected current at the open-circuit voltage (V_{oc}), the device can be turned on and off by

*Address all correspondence to: Zeev Valy Vardeny, E-mail: val@physics.utah.edu

sweeping the external magnetic field to alter the magnetization configuration of the two ferromagnetic (FM) electrodes from parallel to antiparallel. Rather than enhancing the spin aligned current upon illumination, we show that the photocurrent increases the device sensitivity for probing injected spin aligned carriers.

Here, we report the fabrication and characterization of a spin photovoltaic (S-PV) device based on MAPbBr_3 , which is a semiconductor from the HOIPs family. We demonstrate “on and off” current by sweeping the external magnetic field. The voltage dependence and light intensity dependence study indicate that diverging differential magnetocurrent (MC) can be achieved at balanced light intensity and applied bias voltage. We also show that the S-PV device sensitivity may be easily tuned achieving functionalities that are promising in applications, such as magnetic sensing and/or light sensing.

2 Results and Discussion

The S-PV device structure is shown in Fig. 1(a); it is composed of two FM electrodes, namely $\text{La}_{0.67}\text{Sr}_{0.33}\text{MnO}_3$ (LSMO) and Co, and the MAPbBr_3 film as interlayer. The 20-nm semitransparent LSMO film was grown onto $\text{SrTiO}_3(001)$ (STO) substrate by pulsed laser deposition and patterned by photolithography. The MAPbBr_3 was deposited by spin casting from solution. The 0.5-M/litter MAPbBr_3 solution was prepared by mixing 1 : 1.05 MABr and PbBr_2 precursors in dimethyl sulfoxide solvent, following by stirring overnight at 60°C . The LSMO bottom electrode was treated by oxygen plasma for 5 min before putting it into a glove-box (oxygen and water level <1 ppm) for spin coating. The spin coating process was done at 4000 rpm speed for 60 s. Subsequently, the sample was annealed in the glove-box at 110°C for 30 mins. After cooling to ambient temperature, the sample was moved into a vacuum chamber having pressure of

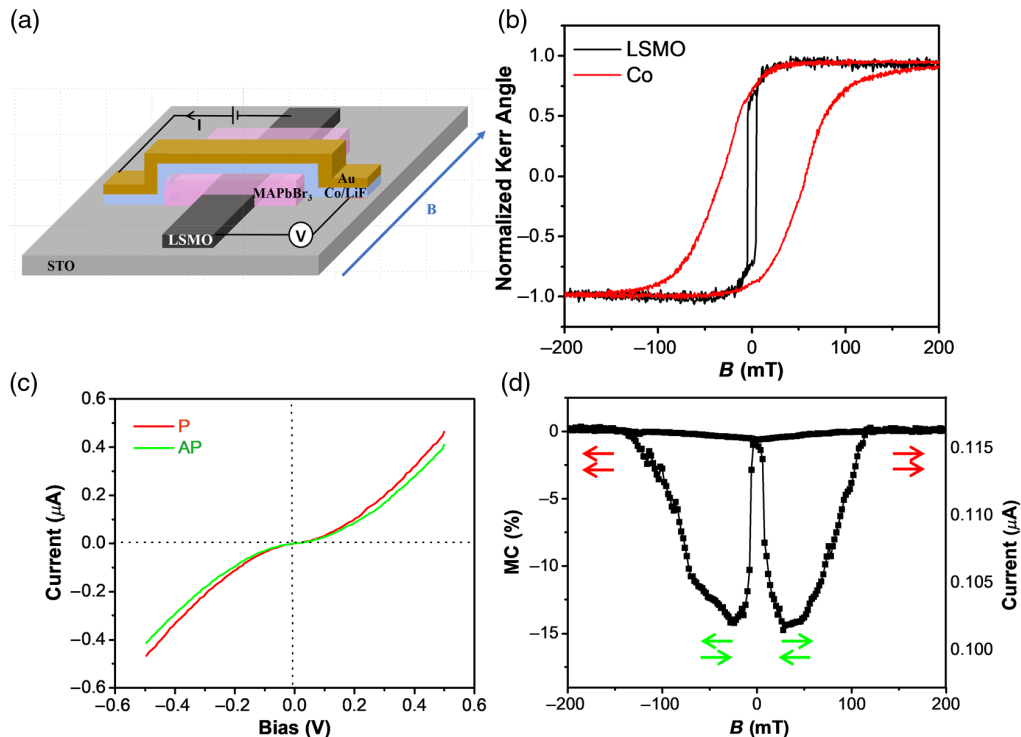


Fig. 1 (a) Schematic illustration of the spin photovoltaic device based on MAPbBr_3 . The LSMO and Co are two FM electrodes with different coercive fields. (b) Normalized Kerr rotation hysteresis loop of LSMO and Co FM electrodes measured *in-situ* by MOKE using a Sagnac interferometer. (c) $I - V$ characteristics of the device at 10 K measured for both parallel (red) and antiparallel (green) magnetization configuration. (d) The current and related MC responses of the spin photovoltaic device measured at 10 K with applied bias voltage of 0.18 V. The respective red and green arrows correspond to parallel and antiparallel magnetization configuration of the FM electrodes.

$<10^{-8}$ Torr for deposition of 1-nm LiF followed by 15-nm Co layer as top electrode. The LiF is employed here to lower the work function of Co in order to form work function difference between Co and LSMO, which may lead to an internal electric field. Finally, a 30-nm gold film was deposited to protect the top electrode from oxidization and water vapor contamination.

The magnetization $M(B)$ hysteresis response of both LSMO and Co electrodes was measured *in-situ* by a homemade Sagnac interferometer¹⁷ having 20-nrad sensitivity and $1\text{-}\mu\text{m}^2$ spot size; the in-plane magnetic field was swept at the same condition as that used for the device performance. As shown in Fig. 1(b), the two FM electrodes show different coercive field, B_c of ~ 5 mT for LSMO and ~ 75 mT for Co. The coercive field difference allows achieving relative magnetization configuration of the two FM electrodes to be parallel or antiparallel to each other by simply sweeping the external magnetic field upward or downward.

The $I - V$ characteristics of the S-PV device at 10 K is illustrated in Fig. 1(c), when the external magnetic field, B is set, respectively, at $B = 200$ mT (parallel configuration of the FM magnetizations) and at $B = -20$ mT (antiparallel configuration). It is clearly seen that the $I - V$ response is different for the two FM magnetization configurations, indicating that the current flow through the device changes depending on the relative orientation of the FM electrode magnetization.^{18,19} This change of current with applied magnetic field is defined as MC, of which value is given by the relation: $\text{MC} = \frac{I_{\text{AP}} - I_{\text{P}}}{I_{\text{P}}} \times 100\%$, where I_{P} and I_{AP} are the currents at parallel and antiparallel magnetization, respectively, measured at the same bias voltage applied to the device. The MC(B) response was measured using four point method with Keithley 236 power supply and Keithley 2000 multimeter.

A substantial MC value of $\sim 15\%$ has been measured in the fabricated S-PV device at 10 K with applied bias of 0.18 V, as shown in Fig. 1(d). As the external magnetic field is swept from positive to negative and vice versa, the current changes according to the magnetization configuration of the two FM electrodes. A difference, ΔI in the injected current in the antiparallel and parallel configuration ($\Delta I = I_{\text{AP}} - I_{\text{P}}$) of 15 nA, is obtained. This result is surprising, since the spin transport in MAPbBr₃ should be ineffective due to its large SOC. The anomalously large spin transport might originate from the Rashba splitting in the conduction band of MAPbBr₃, which may lead to relative long spin diffusion length and spin relaxation time.²⁰

When illumination from a 521-nm diode laser with intensity of 3 mW/cm^2 is applied to the S-PV device from the semitransparent LSMO electrode side, a photovoltaic effect has been observed at 10 K, as shown in Fig. 2. At zero applied bias, a short-circuit current, I_{sc} , of $\sim 0.1 \mu\text{A}$ was measured. Moreover, the obtained $I - V$ characteristics response of the S-PV device under illumination is similar to previously reported HOIP photovoltaic devices [Fig. 2(c)].²¹ The relatively small open-circuit voltage (V_{oc}) indicates that the S-PV device is not ideal for PV application due to the relatively small internal electric field in the device.²² We measured $V_{\text{oc}} = 0.18 \text{ V}$ for the parallel configuration; importantly, the photocurrent in the antiparallel configuration is not null at this applied voltage. Therefore, a current difference, $\Delta I = 15 \text{ nA}$, is measured for the two magnetization configurations, as discussed above. Once the applied voltage is close to V_{oc} in the parallel configuration, the $\text{MC} = \frac{I_{\text{AP}} - I_{\text{P}}}{I_{\text{P}}} \times 100\%$ may be diverging since the denominator, I_{P} , approaches zero. As shown in Fig. 2(d), MC value $> 10,000\%$ can be achieved under these conditions at 10 K.

A schematic view of the S-PV device operation is shown in Figs. 2(a) and 2(b). In the “parallel configuration” [Fig. 2(a)], the electric field applied to the devices equals to the internal photo-induced electric field but in the opposite direction. Therefore, the net current flowing through the device is zero, which is the definition of open-circuit voltage. One can regard the electrical injected current and photo-induced current as two individual channels. Under light illumination condition, the photoexcited electron-hole pairs ionize, resulting in electrons moving to the cathode and holes going to the anode; this generates photocurrent in the device. When the electrical injected current equals the photocurrent but flows in the opposite direction, the two current components cancel each other inside the device so that the external current is null. However, when the external magnetic field is swept leading to antiparallel configuration of the two FM magnetization directions, the electrical injected current becomes smaller [Fig. 2(b)]. By contrast, the photocurrent should not be affected by the magnetization configuration change, and thus remains unchanged. Under this condition, a net current through the device is generated.

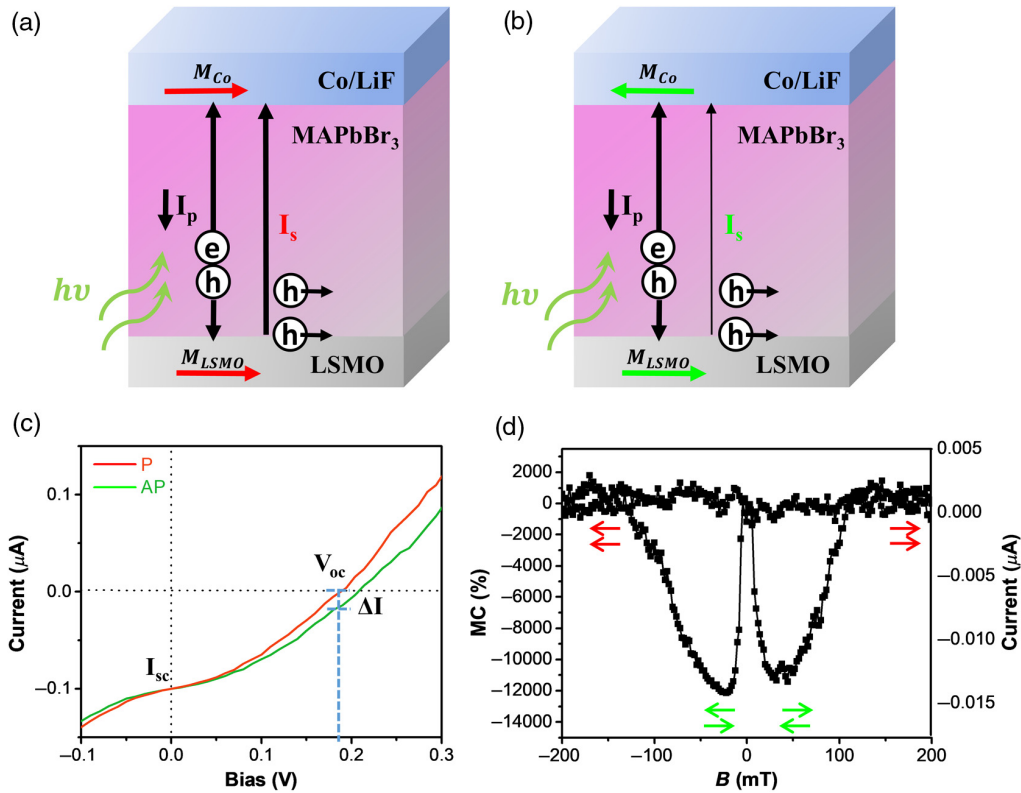


Fig. 2 Schematic of the spin photovoltaic device operation at open-circuit condition, for (a) parallel (in red) and (b) antiparallel (in green) magnetization configuration of the FM electrodes. Note that the spin current, I_s , is smaller in the antiparallel configuration (b), as drawn by a thinner arrow. (c) $I - V$ characteristics of the spin photovoltaic device exposed to light illumination that shows the photovoltaic effect for parallel (red) and antiparallel (green) FM magnetization configuration. (d) $I - B$ and related MC- B responses of the spin photovoltaic device measured at 10 K at bias voltage of 0.18 V, which is the open-circuit voltage of the device at parallel magnetization configuration.

Consequently, the device current changes with the external magnetic field, leading to very large MC when the open-circuit voltage is reached.

Following this “modus operandi,” the current in the device can be turned “on” and “off” by simply sweeping the external magnetic field. This is shown in Fig. 3(a), where the device current is turned “on” in the parallel configuration and “off” in the antiparallel configuration. This device operation has potential functionality for spintronic applications. Other functionalities may be also achieved by controlling the other degree of freedom of the S-PV device. For instance, light intensity, I_L , may affect the device open-circuit voltage (V_{oc} increases with I_L) and therefore influence the magnetic field, where the device switches on. In Fig. 3(b), we show $I - V$ characteristics measured at different I_L from 0 to 3 mW/cm². It can be clearly seen that both I_{sc} and V_{oc} increase monotonically with I_L . In Fig. 3(c), we plot the current change with sweeping magnetic field ($I - B$) measured at constant bias voltage of 0.18 V for different light intensities. It is seen that the baseline current changes via the photovoltaic effect with increasing I_L . When $I_L \approx 3$ mW/cm², the current in the parallel configuration is zero and thus the calculated MC is very large. However, the current difference, ΔI , for parallel and antiparallel stays the same for different I_L values since light irradiation does not affect the electrically injected spin aligned current. Both the measured ΔI and the obtained MC as a function of I_L are plotted in Fig. 4(a). It is clearly seen that ΔI is independent of I_L at fixed bias voltage since the light intensity only modifies the photocurrent. By contrast, since the photocurrent changes with I_L , MC value varies with I_L and diverges at V_{oc} that is set by the light intensity. The large change of the MC value around the diverging point indicates that the device becomes “super sensitive” to changes in I_L and may be used as a sensitive photodetector.

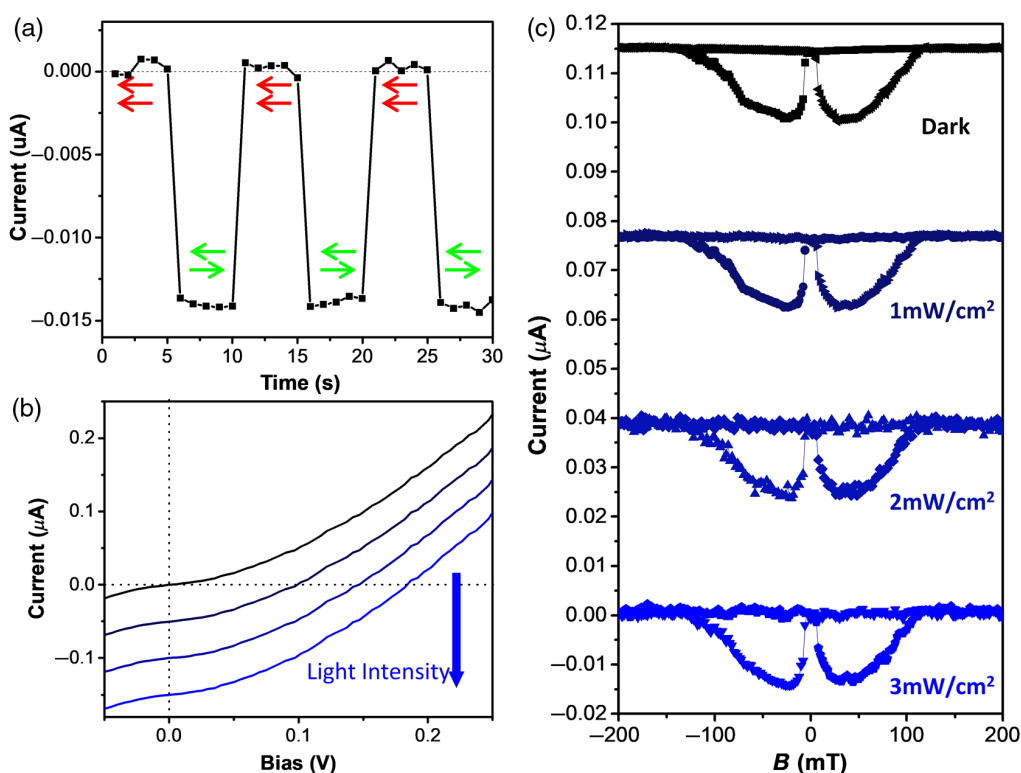


Fig. 3 (a) Switching between “on” and “off” current states of the spin photovoltaic device by sweeping the magnetic field to set the FM magnetization configuration in parallel and antiparallel configuration, respectively, as shown by the horizontal arrows. (b) $I - V$ characteristics of the spin photovoltaic device in the dark, and when exposed to increasing light intensity as denoted by the vertical arrow. (c) $I - B$ response at constant applied bias voltage ($V = 0.18$ V) measured at different light intensities, as given.

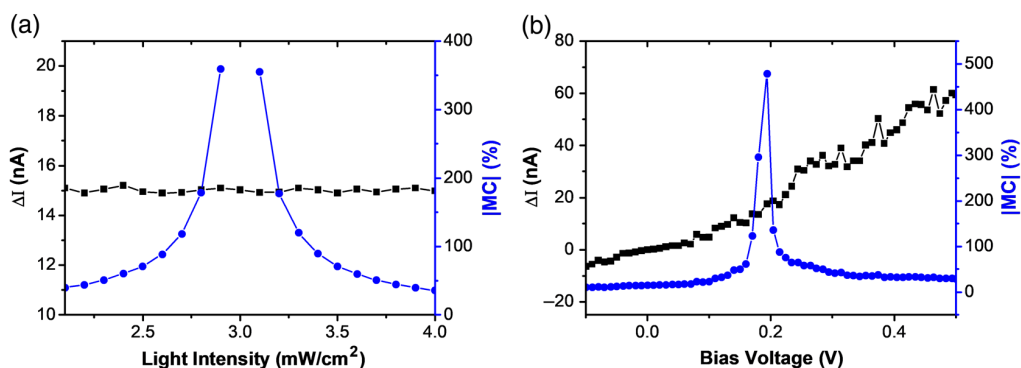


Fig. 4 (a) The measured ΔI (black squares, left axis) and obtained $|MC|$ (blue circles, right axis) plotted as a function of the light illumination intensity applied at fixed bias voltage of 0.18 V. (b) ΔI and $|MC|$ values versus the bias voltage measured at a fixed light illumination intensity of $3\text{ mW}/\text{cm}^2$.

Because of the intermixing between the light illumination intensity and applied voltage, the MC value can be also maximized by tuning the applied bias voltage at a given I_L . To show this functionality, we plot in Fig. 4(b) ΔI and MC as a function of the applied bias voltage at a fixed I_L . The electrically injected spin current is dependent on the spin polarization of the two FM electrodes as well as spin injection efficiency of both interfaces, which are strongly dependent on applied bias voltage.^{23,24} Consequently, ΔI increases with bias voltage. Since I_P also increases with the bias voltage [Fig. 2(c)] and crosses zero at V_{oc} , MC diverges at the open-circuit voltage

set by I_L . The light intensity dependence and bias voltage dependencies of the MC indicate that the device can get incredibly sensitive to even minor change of light intensity and applied voltage as well as external magnetic field close to V_{oc} condition.

Spin injection from FM metals into semiconductor layers is known to be challenging because of the infamous “conductivity mismatch” problem.^{25,26} Therefore, spin injection efficiency in conventional semiconductor-based spin valves has been less than successful, with very limited MC/magnetoresistance value. However, in the S-PV device described here, we can finesse the problem of limited spin injection efficiency into the semiconductor by enhancing the sensitivity of the device using the integration of spin transport and photovoltaic properties. In this scenario, the MC value dramatically increases at V_{oc} . As shown in Fig. 3(a), the switch between zero and nonzero device current for parallel and antiparallel magnetization configurations renders the device useful for complex magnetic and/or light sensor. Moreover, since the base current is set to zero but minor changes in the spin current can be still sensed, the S-PV device should require less energy consumption than traditional spin valves.

3 Conclusion

As a class of semiconductor, the application of HOIPs in the optoelectronics field has developed quickly, reaching limits comparable to those of conventional inorganic photovoltaic materials. This surprising advancement stimulates exploration of other possible application of the HOIPs. In the present work, we propose a spin photovoltaic device based on this emerging material family. Such a device takes advantage of the HOIP excellent optoelectronic properties and efficient spintronic properties, which render its performance better than similar devices based on competing compounds. Due to the intermixing of different degrees of freedom in this device, control over the MC value can be readily achieved. We therefore conclude that the S-PV device paves the way for HOIPs to enter fields other than optoelectronics.

Acknowledgments

This work was supported by the Department of Energy Office of Science under Grant No. DE-SC0014579. The device fabrication facility and C.Z. were supported in part by the National Science Foundation-Material Science & Engineering Center (NSF-MRSEC) program at the University of Utah under Grant No. DMR 1121252. H.G. was supported by the US Department of Energy (DOE) under Grant No. DOE DE-SC0002136.

References

1. M. M. Lee et al., “Efficient hybrid solar cells based on meso-superstructured organometal halide perovskites,” *Science* **338**, 643–647 (2012).
2. M. Liu, M. B. Johnston, and H. J. Snaith, “Efficient planar heterojunction perovskite solar cells by vapour deposition,” *Nature* **501**, 395–398 (2013).
3. W. S. Yang et al., “High-performance photovoltaic perovskite layers fabricated through intramolecular exchange,” *Science* **348**, 1234–1237 (2015).
4. L. Dou et al., “Solution-processed hybrid perovskite photodetectors with high detectivity,” *Nat. Commun.* **5**, 5404 (2014).
5. Q. Dong et al., “Electron-hole diffusion lengths > 175 μm in solution-grown $\text{CH}_3\text{NH}_3\text{PbI}_3$ single crystals,” *Science* **347**, 967–970 (2015).
6. D. Shi et al., “Low trap-state density and long carrier diffusion in organolead trihalide perovskite single crystals,” *Science* **347**, 519–522 (2015).
7. H. Cho et al., “Overcoming the electroluminescence efficiency limitations of perovskite light-emitting diodes,” *Science* **350**, 1222–1225 (2015).
8. M. Kepenekian et al., “Rashba and Dresselhaus effects in hybrid organic-inorganic perovskites: from basics to devices,” *ACS Nano* **9**, 11557–11567 (2015).
9. D. Niesner et al., “Giant Rashba splitting in $\text{CH}_3\text{NH}_3\text{PbBr}_3$ organic-inorganic perovskite,” *Phys. Rev. Lett.* **117**, 126401 (2016).

10. Z.-G. Yu, "Rashba effect and carrier mobility in hybrid organic-inorganic perovskites," *J. Phys. Chem. Lett.* **7**, 3078–3083 (2016).
11. P. Odenthal et al., "Spin-polarized exciton quantum beating in hybrid organic-inorganic perovskites," *Nat. Phys.* **13**, 894–899 (2017).
12. D. Giovanni et al., "Highly spin-polarized carrier dynamics and ultralarge photoinduced magnetization in $\text{CH}_3\text{NH}_3\text{PbI}_3$ perovskite thin films," *Nano Lett.* **15**, 1553–1558 (2015).
13. P. Burrows and S. Forrest, "Electroluminescence from trap-limited current transport in vacuum deposited organic light emitting devices," *Appl. Phys. Lett.* **64**, 2285–2287 (1994).
14. F. Bottegoni et al., "Spin voltage generation through optical excitation of complementary spin populations," *Nat. Mater.* **13**, 790–795 (2014).
15. R. Jansen, "Spintronics: solar spin devices see the light," *Nat. Mater.* **12**, 779–780 (2013).
16. X. Sun et al., "A molecular spin-photovoltaic device," *Science* **357**, 677–680 (2017).
17. J. Xia et al., "Modified Sagnac interferometer for high-sensitivity magneto-optic measurements at cryogenic temperatures," *Appl. Phys. Lett.* **89**, 062508 (2006).
18. M. N. Baibich et al., "Giant magnetoresistance of (001)Fe/(001)Cr magnetic superlattices," *Phys. Rev. Lett.* **61**, 2472–2475 (1988).
19. Z. Xiong et al., "Giant magnetoresistance in organic spin-valves," *Nature* **427**, 821–824 (2004).
20. F. Zheng et al., "Rashba spin-orbit coupling enhanced carrier lifetime in $\text{CH}_3\text{NH}_3\text{PbI}_3$," *Nano Lett.* **15**, 7794–7800 (2015).
21. N. J. Jeon et al., "Compositional engineering of perovskite materials for high-performance solar cells," *Nature* **517**, 476–480 (2015).
22. S. Ryu et al., "Voltage output of efficient perovskite solar cells with high open-circuit voltage and fill factor," *Energy Environ. Sci.* **7**, 2614–2618 (2014).
23. M. Kohda et al., "Bias voltage dependence of the electron spin injection studied in a three-terminal device based on a (Ga,Mn)As/n⁺-GaAs Esaki diode," *Appl. Phys. Lett.* **89**, 012103 (2006).
24. J. M. De Teresa et al., "Role of metal-oxide interface in determining the spin polarization of magnetic tunnel junctions," *Science* **286**, 507–509 (1999).
25. G. Schmidt et al., "Fundamental obstacle for electrical spin injection from a ferromagnetic metal into a diffusive semiconductor," *Phys. Rev. B* **62**, R4790 (2000).
26. E. Rashba, "Theory of electrical spin injection: tunnel contacts as a solution of the conductivity mismatch problem," *Phys. Rev. B* **62**, R16267 (2000).

Jingying Wang received her PhD in physics from North Carolina State University in 2016. She is currently a postdoc researcher working with Prof. Valy Vardeny in the Department of Physics and Astronomy of University of Utah. Her research interest focuses on spintronic properties of organic semiconductor and hybrid perovskite.

Xin Pan received his BS degree in physics from the University of Science and Technology in China. He is now a PhD candidate in the Department of Physics and Astronomy of University of Utah.

Chuang Zhang received his PhD in chemistry from Chinese Academy of Science. He was postdoc working with Prof. Valy Vardeny for three years. Now, he is an assistant professor in the Institute of Chemistry, Chinese Academy of Science.

Hangwen Guo received his PhD from the University of Tennessee and then worked as a postdoc in Louisiana State University. Now, he is an assistant professor of Fudan University in Shanghai, China.

Zeev Valy Vardeny received his PhD in physics from Technion University in 1979. He joined the Department of Physics and Astronomy of University of Utah as a professor in 1987. His research focuses on optical, electrical and magnetic properties of organic semiconductors and other novel materials, as well as devices based on them.